



HAL
open science

Synthesis and Photophysical Characterizations of Pyrroloquinolone Photosensitizers for Singlet Oxygen Production 1

Paul de Bonfils, Catalina Sandoval-Altamirano, Xavier Moreau, Pierrick Nun, Adèle Laurent, German Gunther, Vincent Coeffard

► **To cite this version:**

Paul de Bonfils, Catalina Sandoval-Altamirano, Xavier Moreau, Pierrick Nun, Adèle Laurent, et al.. Synthesis and Photophysical Characterizations of Pyrroloquinolone Photosensitizers for Singlet Oxygen Production 1. *Photochemistry and Photobiology*, 2022, 99 (2), pp.642-651. 10.1111/php.13681 . hal-03779908

HAL Id: hal-03779908


<https://hal.science/hal-03779908>

Submitted on 6 Jun 2023

HAL is a multi-disciplinary open access archive for the deposit and dissemination of scientific research documents, whether they are published or not. The documents may come from teaching and research institutions in France or abroad, or from public or private research centers.

L'archive ouverte pluridisciplinaire **HAL**, est destinée au dépôt et à la diffusion de documents scientifiques de niveau recherche, publiés ou non, émanant des établissements d'enseignement et de recherche français ou étrangers, des laboratoires publics ou privés.

Special Issue Research Article

Synthesis and Photophysical Characterizations of Pyrroloquinolone Photosensitizers for Singlet Oxygen Production[†]Paul De Bonfils^{1*}, Catalina Sandoval-Altamirano², Xavier Moreau³, Pierrick Nun¹, Adèle D. Laurent¹, German Gunther⁴ and Vincent Coeffard^{1*} ¹CNRS, CEISAM, UMR 6230, Nantes Université, Nantes, France²Facultad de Química y Biología, Universidad de Santiago de Chile, Santiago, Chile³UVSQ, CNRS, Institut Lavoisier de Versailles, Université Paris-Saclay, Versailles, France⁴Facultad de Ciencias Químicas y Farmacéuticas, Departamento de Química Orgánica y Físicoquímica, Universidad de Chile, Santiago 1, Chile

Received 31 May 2022, accepted 25 July 2022, DOI: 10.1111/php.13681

ABSTRACT

A series of pyrroloquinolone photosensitizers bearing different halogen substituents (Cl, Br, I) on the heterocyclic framework was studied. These structures were readily prepared through a multi-step synthetic sequence involving an oxidative protocol as an important step to access the quinolone framework. Spectroscopic characterizations and computational investigations were carried out to study the dyes before and after the oxidative step. Interestingly, the fluorescence emission was significantly reduced upon oxidation. In spite of a low photostability under UV light, the pyrroloquinolone photosensitizers proved effective to produce singlet oxygen. Higher singlet oxygen quantum yields were obtained with photosensitizers bearing halogen atoms with a higher atomic number.

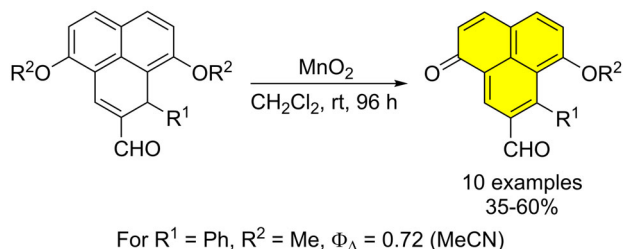
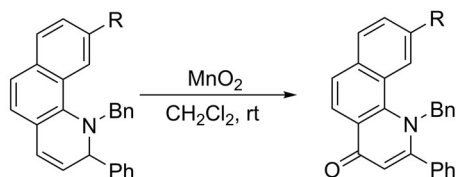
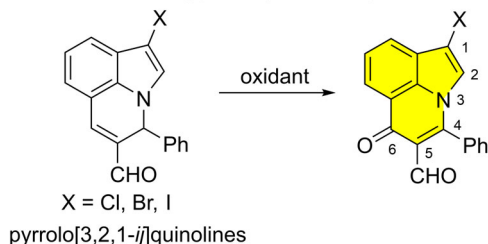
INTRODUCTION

Photosensitization refers to a process by which a photochemical or a photophysical modification occurs in one molecular entity as a result of the absorption of light by another compound called photosensitizer (1). Among the photosensitizing processes, the production of singlet oxygen (¹O₂) by energy transfer from an excited photosensitizer to ground-state oxygen has attracted considerable interest (2–4). Considering the sensitizer triplet excited state (5), the mechanism of oxygen sensitization involves three critical steps: (1) the production of singlet excited states (*S_n*) from the ground state (*S₀*) of the photosensitizer upon ultraviolet or visible light irradiation; (2) the population of the triplet state (*S₁* → *T₁* as a common nonradiative transition) by spin-forbidden intersystem crossing (ISC) which competes with the radiative

fluorescence decay (*S₁* → *S₀*) and nonradiative processes; (3) triplet-triplet energy transfer between the excited photosensitizer and ground state oxygen (6). The high reactivity of singlet oxygen has been harnessed in synthetic chemistry for the production of oxygenated products (7–11), photodynamic therapy (PDT) (12–14) or environmental applications such as water disinfection or pollutant destruction (15). In view of the importance of singlet oxygen, the demand for efficient and readily accessible photosensitizers has been a focus of research efforts in the past decades (16). The efficient generation of singlet oxygen is generally associated with molecules with large intersystem crossing rates (*k_{isc}*) to access the triplet excited state of the photosensitizer. Different strategies are available to populate long-lived triplet states of a photosensitizer such as the introduction of heavy atoms to the chromophore, vibronically assisted ISC, singlet fission, charge recombination mediated triplet formation or twisted induced triplet generation (17). Among the most important organic photosensitizers, 1*H*-phenalen-1-one is considered as a reference sensitizer owing to its high quantum yield of intersystem crossing in a large panel of solvents (18,19). The population of the triplet state occurs *via* a very efficient intersystem crossing between *S₁* (*n*-π*) and *T₁* (π-π*) which follows the El-Sayed's rule (20). In recent years, phenalene photosensitizers have found valuable applications in the photodegradation of wastewater contaminants (21) and in photodynamic therapy for killing bacteria (22–24), fungi (25) and cancer cells (26,27). With the aim of uncovering new methods to prepare functionalized phenalenes, our group reported in 2020 a new class of phenalene photosensitizers for singlet oxygen production (Scheme 1) (28). Our synthetic strategy was based on an unusual oxidative dealkylation of readily available phenalene architectures leading to blue light-absorbing functionalized 6-alkoxy phenalenes. Photophysical characterizations demonstrated that the singlet excited state deactivation was mainly controlled by a nonradiative process such as intersystem crossing. The ability of the phenalene derivatives to produce singlet oxygen was exploited in photooxygenation reactions such as the formation of endoperoxides from aromatics or dienes, and Schenck-ene reactions. In efforts to develop new organic photosensitizers, we envisaged that

*Corresponding authors email: paul.de-bonfils@univ-nantes.fr (Paul De Bonfils) AND vincent.coeffard@univ-nantes.fr (Vincent Coeffard)

[†]This article is part of a Special Issue celebrating the 50th Anniversary of the American Society for Photobiology.© 2022 The Authors. *Photochemistry and Photobiology* published by Wiley Periodicals LLC on behalf of American Society for Photobiology.This is an open access article under the terms of the [Creative Commons Attribution License](https://creativecommons.org/licenses/by/4.0/), which permits use, distribution and reproduction in any medium, provided the original work is properly cited.

a- Our work on the synthesis of phenalenones (2020)**b- Oxidation of phenanthroline core (2007)****c- This work: new pyrroloquinolone photosensitizers****Scheme 1.** Context and concept of this work.

oxidative conditions could be applied to other cyclic frameworks. In 2015, our group described the asymmetric synthesis of enantioenriched pyrrolo[3,2,1-*ij*]quinolines from indole-7-carbaldehyde derivatives through an aminocatalyzed cascade strategy (29). A key element for the success of the organocatalyzed cyclization was the presence of an electron-withdrawing group such as halogens at C-3 position of indole derivatives. With the aim of preparing new photosensitizers, the addition of halogens to the chromophore could also enhance the singlet oxygen quantum yield by increasing the intersystem crossing rate through heavy atom effect (17).

Inspired by a previous study about the oxidation of phenanthroline derivatives into phenanthroline-4-ones (30), and building on our previous work, we reasoned that oxidative conditions could lead to new photosensitizers in light of the propensity of some quinolones to produce singlet oxygen upon illumination (31,32). Besides this application, our strategy will also offer a new synthetic strategy to produce pyrrolo[3,2,1-*ij*]quinolones which are known to elicit various biological activities (33,34). There are several oxidized forms of the pyrrolo[3,2,1-*ij*]quinoline framework such as 4-oxo and 6-oxo-pyrroloquinolines. The 4-oxo-pyrroloquinoline unit is a framework found in natural products and biologically relevant compounds exhibiting anti-fungal (35) or cytotoxic activities (36). In addition, some 4-oxo-pyrroloquinoline derivatives have been found to be selective inhibitors of the aldosterone synthase which is an interesting target for the treatment of hyperaldosteronism, congestive heart failure and myocardial fibrosis (37). Interestingly, the ability of 4-oxo-pyrroloquinoline to produce singlet oxygen under UVA

irradiation has been described by the group of Truscott (38). Contrary to the 4-oxo-pyrroloquinoline framework, 6-oxo-pyrroloquinoline scaffolds appear to be uncommon in natural products. Nevertheless, this unit is the central building block of the antiviral agent PHA-529311 (34,39,40) and some derivatives have demonstrated cytotoxic activities (41). We wish to report herein the synthetic strategy toward new pyrroloquinolone architectures and their photophysical characterization.

MATERIALS AND METHODS

Chemicals and instrumentation. ^1H NMR and ^{13}C spectra were recorded at room temperature on samples dissolved in CDCl_3 . Chemical shifts (δ) are given in parts per million and coupling constants are given as absolute values expressed in Hertz. Structural assignments were made with additional information from gCOSY, gHSQC and gHMBC experiments. High-resolution mass spectrometry (HRMS) analyses were performed using electrospray ionization (ESI) and ASAP. FTIR spectra were obtained from neat samples using the attenuated total reflection (ATR) technique. Thin-layer chromatography (TLC) was carried out on aluminum sheets precoated with silica gel. Column chromatography separations were performed using silica gel. All solvents were of HPLC grade or were distilled using standard drying agents prior to use. Starting chemical substrates and reagents were used as commercially provided unless otherwise indicated.

Synthetic procedures and characterization data. Synthesis of 1-(dibutoxymethyl)-2-nitrobenzene **2**. Under argon atmosphere, 2-nitrobenzaldehyde (3.022 g, 20 mmol, 1 equiv.) was introduced in anhydrous toluene (10 mL). *n*-butan-1-ol (4.58 mL, 50 mmol, 2.5 equiv.) and *p*-toluenesulfonic acid monohydrate (11.2 mg, 60 μmol , 0.003 eq.) were then added. The resulting mixture was left to stir at reflux for 16 h in a flask equipped with a Dean-Stark apparatus. The mixture was cooled down to room temperature and the reaction was quenched with sat. NaHCO_3 (aq.) (40 mL). The mixture was then extracted with ethyl acetate (3 \times 40 mL). The combined organic layers were dried over anhydrous MgSO_4 and the solvent was removed under reduced pressure. The crude compound was purified by column chromatography on silica gel (petroleum ether/EtOAc, 90/10) to afford the corresponding product **2** as a colorless oil (5.23 g, 93%).

^1H (300 MHz, CDCl_3) δ 7.81 ppm (ddd, $J = 7.7, 5.2, 1.4$ Hz, 2H), 7.59 (td, $J = 7.7, 1.4$ Hz, 1H), 7.45 (td, $J = 7.7, 1.4$ Hz, 1H), 6.02 (s, 1H), 3.63 (dt, $J = 9.3, 6.5$ Hz, 2H), 3.52 (dt, $J = 9.2, 6.6$ Hz, 2H), 1.70–1.50 (m, 4H), 1.49–1.25 (m, 4H), 0.91 (t, $J = 7.3$ Hz, 6H). All the physical and spectroscopic data were in complete agreement with the reported ones (42).

Synthesis of 1H-indole-7-carbaldehyde 3. Under argon atmosphere, 1-(dibutoxymethyl)-2-nitrobenzene **2** (2.532 g, 9 mmol, 1 equiv.) was introduced in anhydrous tetrahydrofuran (30 mL). The solution was cooled down to 221245°C . Vinylmagnesium bromide (1 M in THF, 29.7 mL, 29.7 mmol, 3.3 equiv.) was added dropwise (2 mL $\cdot\text{min}^{-1}$). The mixture was then left to stir for 45 min at -45°C . The mixture was allowed to warm to room temperature and 1 M HCl (aq.) (29.7 mL, 3.3 equiv.) was carefully added and the resulting mixture was stirred for 45 min at room temperature. The reaction was then neutralized with sat. NaHCO_3 aq. (30 mL) and then extracted with Et_2O (3 \times 30 mL). The combined organic layers were dried over anhydrous MgSO_4 and the solvent was removed under reduced pressure. The crude compound was purified by column chromatography on silica gel (petroleum ether/ CH_2Cl_2 , 70/30) to afford the corresponding product **3** as a pale yellow solid (848.9 mg, 65%).

^1H (300 MHz, CDCl_3) δ 10.17 ppm (br s, 1H), 10.13 (s, 1H), 7.95 (dt, $J = 7.8, 1.1$ Hz, 1H), 7.67 (dd, $J = 7.8, 1.1$ Hz, 1H), 7.36 (dd, $J = 3.3, 2.2$ Hz, 1H), 7.28 (dd, $J = 7.8, 7.3$ Hz, 1H), 6.64 (dd, $J = 3.3, 2.2$ Hz, 1H). All the physical and spectroscopic data were in complete agreement with the reported ones (42).

General procedure for the synthesis of 1H-indole-7-carbaldehyde derivatives 4a and 4b. Under argon atmosphere, 1H-indole-7-carbaldehyde **3** (1 equiv.) was introduced in anhydrous dichloromethane (0.2 mol $\cdot\text{L}^{-1}$). *N*-chlorosuccinimide (NCS) (1.2 equiv.) or *N*-bromosuccinimide (NBS) (1 equiv.) was then added in one portion. The resulting mixture was left to stir for 3–4 h at room temperature. The

reaction was monitored by TLC (petroleum ether/EtOAc, 85/15). After completion of the reaction, water was added. The aqueous phase was extracted three times with dichloromethane. The combined organic layers were dried over anhydrous MgSO₄ and the solvent was removed under reduced pressure. The crude compound was purified by column chromatography on silica gel (petroleum ether/EtOAc, 85/15) to afford the corresponding product as a solid.

3-chloro-1H-indole-7-carbaldehyde 4a. According to the general procedure, 608.7 mg (82%) of **4a** (pale yellow solid) was obtained from 1H-indole-7-carbaldehyde **3** (600 mg, 4.13 mmol) and *N*-chlorosuccinimide (288.1 mg, 4.96 mmol). ¹H (300 MHz, CDCl₃) δ 10.07 ppm (s, 1H), 9.97 (br s, 1H), 7.89 (dt, *J* = 7.8, 1.0 Hz, 1H), 7.66 (ddd, *J* = 7.8, 1.0, 0.4 Hz, 1H), 7.31–7.20 (m, 2H). All the physical and spectroscopic data were in complete agreement with the reported ones (29).

3-bromo-1H-indole-7-carbaldehyde 4b. According to the general procedure, 562.7 mg (91%) of **4b** (pale yellow solid) was obtained from 1H-indole-7-carbaldehyde **3** (400 mg, 2.76 mmol) and *N*-bromosuccinimide (490.4 mg, 2.76 mmol). ¹H (300 MHz, CDCl₃) δ 10.12 ppm (s, 1H), 7.89 (dt, *J* = 7.9, 1.1 Hz, 1H), 7.73 (dd, *J* = 7.4, 1.1 Hz, 1H), 7.41–7.32 (m, 2H). All the physical and spectroscopic data were in complete agreement with the reported ones (29).

Synthesis of 3-iodo-1H-indole-7-carbaldehyde 4c. Under argon atmosphere, 1H-indole-7-carbaldehyde **3** (500 mg, 3.44 mmol, 1 equiv.) was introduced in anhydrous *N,N*-dimethylformamide (9.8 mL). KOH (483.1 mg, 8.61 mmol, 2.5 equiv.) and I₂ (1.75 g, 6.89 mmol, 2 equiv.) were successively added. The reaction was left to stir at room temperature for 2 h, at which point a sat. Na₂S₂O₃ (aq.) (30 mL) was added. The aqueous phase was extracted with dichloromethane (3 × 15 mL) and the combined organic layers were washed with brine (2 × 100 mL). The organic layer was dried over anhydrous MgSO₄ and the solvent was removed under reduced pressure. The crude compound was purified by column chromatography on silica gel (cyclohexane/EtOAc, 85/15) to afford the corresponding product **4c** as a pale orange solid (691.1 mg, 74%).

R_f = 0.47 (cyclohexane/EtOAc, 85/15). M.p. 121–123°C. ¹H (300 MHz, CDCl₃) δ 10.28 ppm (br s, 1H), 10.10 (s, 1H), 7.76 (dt, *J* = 7.9, 1.0 Hz, 1H), 7.72 (dd, *J* = 7.3, 1.0 Hz, 1H), 7.43 (d, *J* = 2.4 Hz, 1H), 7.36 (dd, *J* = 7.9, 7.3 Hz, 1H). ¹³C NMR (75 MHz, CDCl₃) δ 193.3 ppm, 133.8, 131.2, 130.4, 129.9, 128.5, 120.8, 120.4, 57.9. IR (ATR, cm⁻¹) 3332, 3118, 3054, 2804, 1790, 1667, 1607, 1588, 1097, 530. HRMS (ASAP+) *m/z*: [M + H]⁺ calcd for C₉H₇INO 271.9572; found 271.9577.

General procedure for the synthesis of pyrroloquinoline derivatives 5a and 5b. The indole substrate **4a** or **4b** (1 equiv.) was introduced in chloroform filtered over alumina (0.2 mol L⁻¹). Sodium acetate (1.1 equiv.), a racemic mixture of diphenylprolinol silyl ether catalyst (15 mol %) and *trans*-cinnamaldehyde (1.5 equiv.) were successively added. The reaction mixture was left to stir at 55°C for 40 h, at which point the solvent was removed under reduced pressure. The crude compound was purified by column chromatography to afford the corresponding product as a solid.

1-chloro-4-phenyl-4H-pyrrolo[3,2,1-*ij*]quinoline-5-carbaldehyde 5a. According to the general procedure, 705.9 mg (79%) of **5a** (pale yellow solid) was obtained from 3-chloro-1H-indole-7-carbaldehyde **4a** (547 mg, 3.05 mmol), sodium acetate (275.6 mg, 3.36 mmol), diphenylprolinol silyl ether catalyst (149.7 mg, 0.46 mmol) and *trans*-cinnamaldehyde (0.58 mL, 4.58 mmol). The compound was purified by column chromatography on silica gel (petroleum ether/EtOAc, 85/15), and if necessary by a second column chromatography on silica gel (cyclohexane/PhCH₃, 10/90). ¹H (300 MHz, CDCl₃) δ 9.50 ppm (s, 1H), 7.60 (dd, *J* = 8.0, 1.0 Hz, 1H), 7.50 (d, *J* = 1.0 Hz, 1H), 7.21–7.20 (m, 1H), 7.19–7.17 (m, 3H), 7.12–7.07 (m, 3H), 6.89 (s, 1H), 6.43 (s, 1H). All the physical and spectroscopic data were in complete agreement with the reported ones (29).

1-bromo-4-phenyl-4H-pyrrolo[3,2,1-*ij*]quinoline-5-carbaldehyde 5b. According to the general procedure, 612.2 mg (65%) of **5b** (pale yellow solid) was obtained from 3-bromo-1H-indole-7-carbaldehyde **4b** (500 mg, 2.23 mmol), sodium acetate (201.0 mg, 2.45 mmol), diphenylprolinol silyl ether catalyst (108.9 mg, 0.33 mmol) and *trans*-cinnamaldehyde (0.42 mL, 3.35 mmol). The compound was purified by column chromatography on silica gel (petroleum ether/EtOAc, 85/15), and if necessary by a second column chromatography on silica gel (cyclohexane/PhCH₃, 10/90). ¹H (300 MHz, CDCl₃) δ 9.61 ppm (s, 1H), 7.70–7.56 (m, 2H), 7.35–7.29 (m, 5H), 7.24–7.19 (m, 2H), 7.07 (s, 1H), 6.56 (s,

1H). All the physical and spectroscopic data were in complete agreement with the reported ones (29).

General procedure for the synthesis of pyrroloquinoline derivatives 6a and 6b. The pyrroloquinoline substrate (1 equiv.) was introduced in dichloroethane (0.1 mol L⁻¹). Osmotic water (2 equiv.) and 2,3-dichloro-5,6-dicyano-1,4-benzoquinone (DDQ) (2 equiv.) were successively added. The reaction mixture was left to stir at 60°C for 2 h, at which point water was added. The aqueous phase was extracted three times with dichloromethane. The combined organic layers were dried over anhydrous MgSO₄ and the solvent was removed under reduced pressure. The crude compound was purified by column chromatography on silica gel (*n*-pentane/EtOAc, 70/30) to afford the corresponding product as a solid.

1-chloro-6-oxo-4-phenyl-6H-pyrrolo[3,2,1-*ij*]quinoline-5-carbaldehyde 6a. According to the general procedure, 269.8 mg (91%) of **6a** (pale yellow solid) was obtained from 1-chloro-4-phenyl-4H-pyrrolo[3,2,1-*ij*]quinoline-5-carbaldehyde **5a** (280 mg, 0.955 mmol), osmotic water (34.4 μL, 1.91 mmol) and DDQ (433.6 mg, 1.91 mmol). *R_f* = 0.45 (*n*-pentane/EtOAc, 70/30). M.p. decomposition. ¹H (300 MHz, CDCl₃) δ 10.29 (s, 1H), 8.32 (ddd, *J* = 7.8, 1.0, 0.5 Hz, 1H), 7.98 (dd, *J* = 7.8, 1.0 Hz, 1H), 7.69 (t, *J* = 7.8 Hz, 1H), 7.65–7.55 (m, 3H), 7.48–7.44 (m, 2H), 6.98 (s, 1H). ¹³C NMR (75 MHz, CDCl₃) δ 190.1 ppm, 178.7, 153.1, 134.1, 131.0, 129.7, 129.2 (2C), 129.0 (2C), 128.2, 126.6, 125.7, 124.5, 123.7, 122.4, 119.9, 118.6. IR (ATR, cm⁻¹) 3151, 3049, 2843, 1699, 1687, 1642, 1621, 1063, 751. HRMS (ASAP+) *m/z*: [M + H]⁺ calcd for C₁₈H₁₁ClNO₂ 308.0478; found 308.0480.

1-bromo-6-oxo-4-phenyl-6H-pyrrolo[3,2,1-*ij*]quinoline-5-carbaldehyde 6b. According to the general procedure, 311.1 mg (85%) of **6b** (pale yellow solid) was obtained from 1-bromo-4-phenyl-4H-pyrrolo[3,2,1-*ij*]quinoline-5-carbaldehyde **5b** (350 mg, 1.04 mmol), osmotic water (37.5 μL, 2.08 mmol) and DDQ (472.2 mg, 2.08 mmol). *R_f* = 0.45 (*n*-pentane/EtOAc, 70/30). M.p. decomposition. ¹H (300 MHz, CDCl₃) δ 10.30 ppm (s, 1H), 8.32 (dd, *J* = 7.5, 0.8 Hz, 1H), 7.91 (dd, *J* = 7.5, 0.8 Hz, 1H), 7.69 (t, *J* = 7.5 Hz, 1H), 7.67–7.57 (m, 3H), 7.49–7.44 (m, 2H), 7.04 (s, 1H). ¹³C (75 MHz, CDCl₃) δ 190.1 ppm, 178.7, 152.9, 134.5, 131.0, 129.7 (2C), 129.2 (2C), 129.0 (2C), 126.6, 126.5, 124.8, 124.4, 123.7, 119.9, 104.2. IR (ATR, cm⁻¹) 3145, 3045, 2855, 1698, 1641, 1621, 1595, 1052, 581. HRMS (ASAP+) *m/z*: [M + H]⁺ calcd for C₁₈H₁₁BrNO₂ 351.9973; found 351.9976.

Synthesis of 1-iodo-6-oxo-4-phenyl-6H-pyrrolo[3,2,1-*ij*]quinoline-5-carbaldehyde 6c. *Step 1.* 3-iodo-1H-indole-7-carbaldehyde **4c** (500 mg, 1.84 mmol, 1 equiv.) was introduced in chloroform filtered over alumina (9.2 mL). Sodium acetate (165.7 mg, 2.02 mmol, 1.1 equiv.), a racemic mixture of diphenylprolinol silyl ether catalyst (91 mg, 0.28 mmol, 15 mol %) and *trans*-cinnamaldehyde (0.35 mL, 2.76 mmol, 1.5 equiv.) were successively added. The reaction mixture was left to stir at 55°C for 40 h, at which point the solvent was removed under reduced pressure. The excess of the *trans*-cinnamaldehyde was removed by column chromatography (cyclohexane/PhCH₃, 10/90). Despite extensive efforts the separation of the substrate and the desired product was unsuccessful. The conversion was determined by ¹H NMR in the crude compound (27%). The crude compound was used in the next step without further purification. *Step 2.* The crude compound (192 mg, 0.50 mmol, 1 equiv.) was introduced in dichloroethane (2.5 mL). Osmotic water (18 μL, 1 mmol, 2 equiv.) and 2,3-dichloro-5,6-dicyano-1,4-benzoquinone (DDQ) (227 mg, 1 mmol, 2 equiv.) were successively added. The reaction mixture was left to stir at 60°C for 2 h, at which point water was added. The aqueous phase was extracted three times with dichloromethane. The combined organic layers were dried over anhydrous MgSO₄ and the solvent was removed under reduced pressure. The crude compound was purified by column chromatography on silica gel (*n*-pentane/EtOAc, 70/30) to afford the corresponding product **6c** as a pale yellow solid (162 mg, 22% overall yield).

R_f = 0.47 (*n*-pentane/EtOAc, 7/3). M.p. decomposition. ¹H (400 MHz, CDCl₃) δ 10.32 ppm (s, 1H), 8.32 (dd, *J* = 7.7, 1.0 Hz, 1H), 7.77 (dd, *J* = 7.7, 1.0 Hz, 1H), 7.69 (t, *J* = 7.7 Hz, 1H), 7.66–7.55 (m, 3H), 7.49–7.44 (m, 2H), 7.10 (s, 1H). ¹³C (100 MHz, CDCl₃) δ 190.2 ppm, 178.7, 152.4, 134.9, 132.7, 131.0, 129.8, 129.7, 129.3 (2C), 129.0 (2C), 128.1, 126.6, 124.3, 123.7, 119.7, 71.1. IR (ATR, cm⁻¹) 3137, 3047, 2923, 2850, 1735, 1697, 1641, 1620, 1452, 1262, 538. HRMS (ASAP+) *m/z*: [M + H]⁺ calcd for C₁₈H₁₁INO₂ 399.9834; found 399.9837.

Spectroscopic and photophysical measurements. UV–Vis spectra were recorded on an Agilent 8453 Diode-Array spectrophotometer in the range of 250–700 nm. Emission spectra were measured in an ISS PCI

spectrofluorometer at room temperature. Luminescence lifetime measurements were carried out using a PicoQuant FluoTime 200 fluorescence lifetime spectrometer with a multichannel scaler (PicoQuant's Timeharp 250) with the time correlated single photon counting (TCSPC) method. A 375 nm laser LDHPC375 (Picoquant) pulsed at 10 or 20 MHz was employed as an excitation source. Lifetimes were obtained from global fit of at least 25 decays obtained at different emission wavelengths.

Fluorescence quantum yields were determined using Eq. (1) and 6-ethoxy-phenalene in acetonitrile ($\Phi_F = 0.049$) and chloroform ($\Phi_F = 0.018$) as reference (43)

$$\Phi_{F,\text{sample}} = \Phi_{F,\text{reference}} \frac{A_{\text{reference}}}{A_{\text{sample}}} \frac{I_{\text{sample}}}{I_{\text{reference}}} \left(\frac{\eta_{\text{sample}}}{\eta_{\text{reference}}} \right)^2 \quad (1)$$

Φ_F is the fluorescence quantum yield, A is the absorbance in the wavelength of excitation, I corresponds to area of the emission spectra and η is the refractive index of the solvent.

For consumption kinetic experiences, irradiation was achieved with LED M365LP1 at 365 nm (Thorlabs), working at 100% power.

Lifetime decays of singlet oxygen, $O_2(^1\Delta_g)$, were acquired with a FluoTime 200 consisting in a multichannel scaler Nanoharp 200. Excitation at 355 nm was achieved with a laser FTSS355-Q3 (Crystal Laser, Berlin, Germany) working at 1 kHz repetition rate. For the detection at 1270 nm a NIR PMT H10330A (Hamamatsu) was employed. The $O_2(^1\Delta_g)$ quantum yields (Φ_Δ) were determined by comparing the intensity at zero time of the 1270 nm signals to those of optically matched solutions of phenalene as reference, according to the following equation. We used fresh solution for each measurement and short times of irradiation to minimize photodecomposition. Integrity of samples was checked after measurement (19):

$$\Phi_\Delta = \frac{I_\Delta(t=0)}{I'_\Delta(t=0)} \Phi'_\Delta$$

Photodegradation quantum yields (Φ_D) were determined using the following equation:

$$\phi_D = \frac{d[P]/dt}{I_a} V$$

where $d[P]/dt$ is the photooxidation rate (related with absorbance decrease around 370 nm, and expressed in concentration per time units), V is the solution volume and I_a is the photon flux determined by 9,10-dimethylanthracene self-sensitized photooxygenation followed at 324 nm.

Computational details. All calculations were carried out with Gaussian 16 software (44) using density functional theory (DFT) and its time-dependent counterpart (TD-DFT) for **5a** and **6a**. We considered acetonitrile and chloroform for absorption properties and only acetonitrile for emission as the solvent effects are trifling on fluorescence properties according to the photophysical experiments. First geometries optimization and frequencies were calculated both in the ground state and excited state using the M06-2X metageneralized gradient approximation hybrid exchange-correlation functional (45) combined to the Pople 6-31G(d) basis set. The solvent effects have been included through the Pisa Polarizable Continuum Model (PCM) (46). Second, TD-DFT calculations have been carried out accounting for the solvent responses in its nonequilibrium regime through corrected Linear Response Model (cLR) (47) using a large basis set, 6-311 + G(2d,p). For oxidized forms, Singlet-Triplet energy gap (ΔE_{ST}) has been estimated with the higher-level Spin-Component Scaling second-order approximate Coupled-Cluster (SCS-CC2) with the Def2-DZVP basis in gas phase with Turbomole (TURBOMOLE V7.3, a development of University of Karlsruhe and Forschungszentrum Karlsruhe GmbH, 1989–2007; TURBOMOLE GmbH) while the spin-orbit coupling (SOC) values reported in the main text were determined as $\sqrt{\frac{1}{3}S_x^2 + \frac{1}{3}S_y^2 + \frac{1}{3}S_z^2}$. The elements of the SOC matrix were estimated in ORCA 5.2 (48) software using M06-2X/def2-TZVP level of theory in acetonitrile except for **6c** as not implemented in case of pseudopotential (SMD solvation model). The RI-SOMF(1X) was used for speeding up the calculation time with only a small error associated (49).

RESULTS AND DISCUSSION

Synthesis of the photosensitizers

At the outset of this work, a range of halogen-containing pyrrolo [3,2,1-*ij*]quinolines **5a-c** was prepared based on our previous studies (Scheme 2) (29).

The synthesis started with the formation of acetal **2** from the commercially available 2-nitrobenzaldehyde **1**. Under acid catalysis, acetalization of aldehyde **1** in the presence of *n*-butanol afforded the product **2** in 93% isolated yield. The Bartoli indole synthesis from the nitro derivative **2** and vinylmagnesium bromide gave rise to **3** in 65% yield after an aqueous work up (50). Halogenation of the indole nucleus was carried in the presence of *N*-chlorosuccinimide (NCS) or *N*-bromosuccinimide (NBS) to afford respectively **4a** in 82% yield and **4b** in 91% yield. The 3-iodo indole derivative **4c** was prepared by iodination of **3** in the presence of iodine and the resulting product **4c** was isolated in 74% yield. The formation of the pyrrolo[3,2,1-*ij*]quinoline framework was then performed in the presence of a racemic mixture of the Hayashi-Jørgensen catalyst through an iminium-enamine strategy (29). Starting from *trans*-cinnamaldehyde, the chloro- and bromo-derivatives **5a** and **5b** were isolated in 79% and 65% yields, respectively. The reaction of **4c** and *trans*-cinnamaldehyde led to an inseparable mixture of **4c/5c** which was used in the subsequent oxidative step. A conversion of 27% was determined by ^1H NMR on the crude (see **Materials and Methods** for further details). With the compounds **5a-c** in hand, the oxidative conditions were then investigated (Table 1).

Initial attempts to oxidize **5a** revealed that MnO_2 was a suitable oxidant to form **6a** in 65% yield (entry 1). The structure of **6a** was elucidated using extensive 1D and 2D NMR spectroscopy and further conditions were screened in order to increase the reaction yields. Addition of 2 equiv. of water had a negative impact on the yield and the product **6a** was isolated in 24% yield (entry 2). Oxidation in the presence of nitrosyl tetrafluoroborate (NOBF_4) at room temperature did not produce the desired product and only side products were detected in the crude mixture (entry 3). The ability of rose bengal to oxidize benzylic position bearing a nitrogen functionality was applied to the oxidation of **5a** but no reaction occurred (entry 4) (51). A similar result was also observed by using 2,3-dichloro-5,6-dicyano-1,4-benzoquinone (DDQ) in 1,2-dichloroethane at 60°C (entry 5). The combination of water and DDQ has proved successful for the oxidation of allylic aromatic derivatives into the corresponding cinnamaldehydes (52) and these conditions were tested for forming **6a** (entry 6). The addition of 2 equiv. of water had a dramatic impact on the reaction yield by producing **6a** in 91% yield in only 2 h reaction time. With optimal reaction conditions in hand, the formation of **6a-c** was investigated (Scheme 3).

The oxidative conditions were applied to **5a** and **5b** and the products **6a** and **6b** were obtained in excellent yields of 91% and 85%, respectively. As described above, the intermediate **5c** could not be isolated in pure form from **4c** after the aminocatalyzed step and the mixture was oxidized under the optimized conditions leading to **6c** in 22% isolated yield over two steps.

Photophysical characterizations and computational analyses

Steady-state absorption and emission spectra. The absorption spectra and molar absorption coefficients of the chromophores **5a**

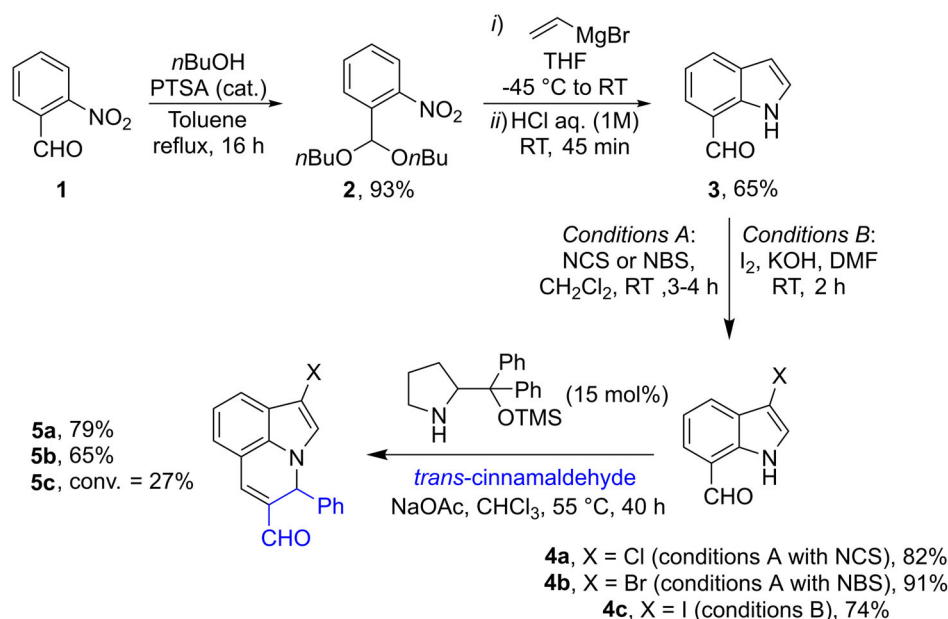
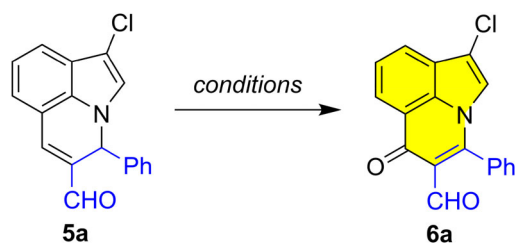
Scheme 2. Synthesis of pyrrolo[3,2,1-*ij*]quinolines **5a-c**.

Table 1. Screening of oxidation conditions.

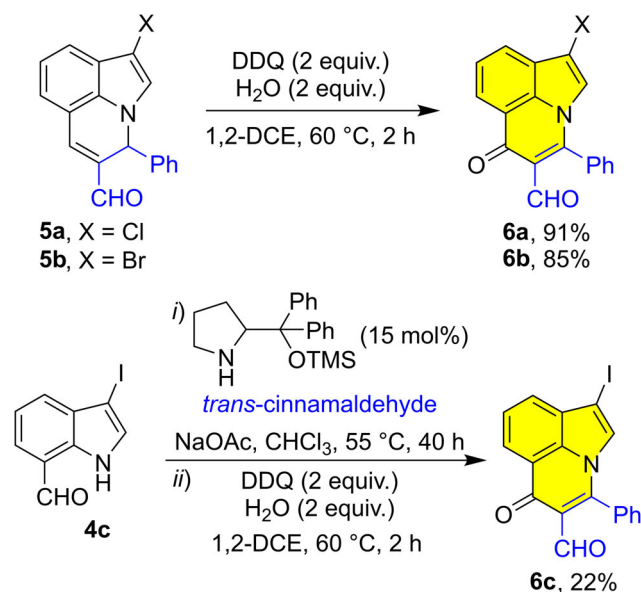


Entry	Conditions*	Yield (Conv.)
1	MnO ₂ (20 equiv.), CH ₂ Cl ₂ , 48 h, RT	65% (80%)
2	MnO ₂ (20 equiv.), H ₂ O (2 equiv.), CH ₂ Cl ₂ , 48 h, RT	24% (28%)
3	NOBF ₄ (2 equiv.), MeCN, 5 min, RT	– [†]
4	Rose bengal (2 mol%), MeOH, green LED, 2 h, RT	0% [‡] (0%)
5	DDQ (2 equiv.), 1,2-DCE, 2 h, 60 °C	0% [‡] (0%)
6	DDQ (2 equiv.), H ₂ O (2 equiv.), 1,2-DCE, 2 h, 60 °C	91% (100%)

*For the procedures, see the Supporting Information. [†]Decomposition of the starting material. [‡]No reaction.

and **6a-c** were investigated in two solvents of different polarities, acetonitrile and chloroform (Fig. 1 and Table 2).

The absorption spectra of **5a** and the oxidized compound **6a** showed noticeable differences. The oxidation of **5a** caused a 22 nm hypsochromic shift in acetonitrile. Such a shift has been reproduced by theoretical calculation (see [Materials and Methods](#) for computational details) using time-dependent density functional theory (Table 2). For **5a** the S₀→S₁ electronic transition (384 nm) was characterized by a π→π* (Fig. 1) with a large oscillator strength (*f* = 0.27) while the oxidized form behaved differently. Indeed, the first bright state corresponded to a S₀→S₃

Scheme 3. Formation of **6a-c**.

electronic transition (330 nm, *f* = 0.27) in acetonitrile, the first two lowest transitions being *n*→π* are forbidden by selection rules. The electronic density difference plot (Fig. 1) of **5a** and **6a** depicted a common π→π* character but with a less extended π-delocalization when the carbonyl group is present explaining the blue-shift. Upon photoexcitation a gain of electronic density (green zone in Fig. 2) was observed on the aldehyde function of **5a** while not in **6a** as it is out-of-plane (see Supporting Information for further details). The molar extinction coefficients (*ε*) were determined in acetonitrile and chloroform and the results are depicted in Table 2.

The absorption spectra (maximum wavelengths) were slightly influenced by the nature of the halogen borne by the indole nucleus in chloroform and acetonitrile, but higher molar

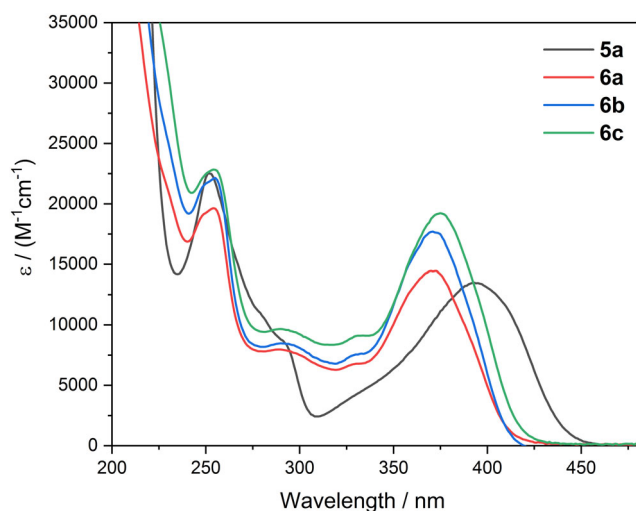


Figure 1. Absorption spectra of **5a** and **6a-c** in acetonitrile.

Table 2. Molar extinction coefficients determined in selected solvents (ϵ , $M^{-1} \text{ cm}^{-1}$) and measured maximum absorption wavelength (λ_{max}). Computed oscillator strength (f) and λ_{max} at the M06-2X-6-311 + G(2d,p) level of theory using PCM solvent and the cLR² to account for the electronic response of the solvent.

Compound	Experiment		Theory	
	$\epsilon/M^{-1} \text{ cm}^{-1} (\lambda_{\text{max}}/\text{nm})$		$f (\lambda_{\text{max}}/\text{nm})$	
	MeCN	CHCl ₃	MeCN	CHCl ₃
5a	13 657 (392)	13 691 (405)	0.27 (384)	0.29 (384)
6a	14 411 (370)	14 202 (373)	0.27 (330)	0.31 (331)
6b	17 213 (371)	23 446 (373)	0.28 (331)	0.32 (332)
6c	19 714 (375)	19 875 (373)	0.27 (335)	0.32 (335)

absorption coefficients were measured for **6c** containing an iodine atom than the chloro-substituted compound **6a** in acetonitrile. Concerning the oxidized forms, theoretical computations

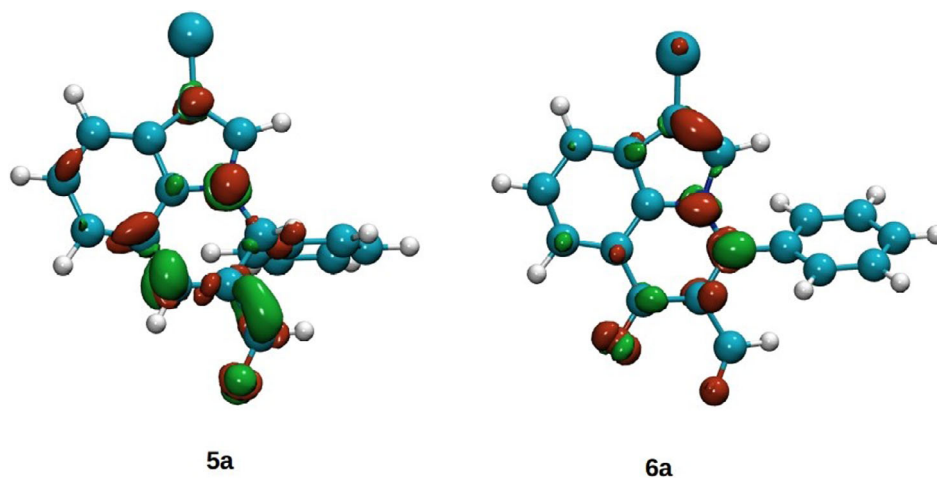


Figure 2. Electron density plots of **5a** and **6a**. Red and green lobes correspond, respectively, to a decrease and increase of electron density upon absorption. Contour: 0.004.

are in the line with experiments with a very small red-shift going from **6a** to **6c**. Normalized emission spectra in acetonitrile of **5a** and **6a-c** are shown in Fig. 3.

For the pyrrolo[3,2,1-*ij*]quinoline **5a**, the emission band in acetonitrile was centered around 510 nm while the emission maxima for **6a**, **6b** and **6c** derivatives were located around 460 nm. The measured Stokes shift for **5a** in acetonitrile (118 nm) is in good agreement with theoretical calculation (126 nm). As can be seen in Fig. 2 and according to the fluorescence quantum yields reported in Table 3, emission intensity of **5a** was high while the low emission of the oxidized derivatives **6a-c** allowed to consider these structures as nonfluorescent chromophores.

Fluorescence quantum yields were measured under air ($\Phi_{F,\text{air}}$) and under argon ($\Phi_{F,\text{Ar}}$) for all studied compounds (Table 3). Despite being low, the similarity between the reported values indicates that oxygen is not able to quench appreciably the singlet states of these derivatives. Additionally, fluorescence quantum yields for the derivatives **6** showed a clear inverse dependence with the atomic weight of halogen substituent, as reported for heterocyclic compounds such as Bodipy derivatives (53,54) or quinoxaline-based chromophores (55) substituted with halogen atoms.

Time-resolved measurements. For **5a**, fluorescence lifetime data were analyzed by global fitting of a set of decays acquired at different emission wavelengths, with excitation at 375 nm. A representative data analysis showing a mono-exponential fit in acetonitrile gave a lifetime of 6.4 ns. The results and fitting are shown in Fig. 4. Lifetime measurements after argon bubbling yielded a very similar result (6.9 ns), indicating, as previously mentioned, a negligible quenching by oxygen. For compounds **6a-c**, their lifetimes were not measured, considering their low emission quantum yields.

Photostability studies. The analyses were carried out in acetonitrile on samples of **5a** and **6a-c** by monitoring the changes in absorbance at different peak positions upon irradiation at 365 nm for 10 min (see Materials and Methods for further information). The chromophore **5a** was stable under these conditions while the

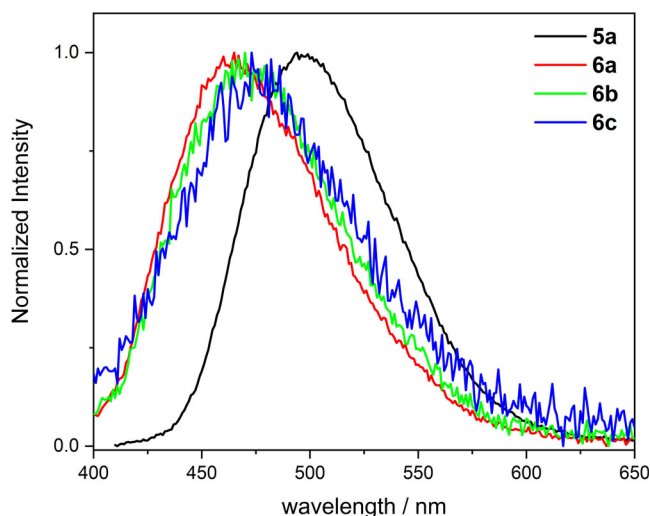


Figure 3. Normalized emission spectra of **5a** and **6a-c** in acetonitrile. $\lambda_{\text{exc}} = 375$ nm.

Table 3. Fluorescence quantum yields.

Compound	MeCN		CHCl ₃	
	$\Phi_{\text{F,air}}$	$\Phi_{\text{F,Ar}}$	$\Phi_{\text{F,air}}$	$\Phi_{\text{F,Ar}}$
5a	0.358	0.359	0.263	0.270
6a	0.007	0.011	0.002	0.003
6b	0.004	0.003	0.001	0.001
6c	0.002	0.001	–	0.001

oxidized compounds **6a-c** had a different behavior (Fig. 5). With compounds **6a-c**, a relative fast decrease of the absorption band at the maximum wavelength with time was observed and this instability was confirmed by examining the evolution of other absorption bands. The photodegradation quantum yields at 365 nm for **6a-c** were $\Phi_{\text{D}} = 0.030$ (**6a**), $\Phi_{\text{D}} = 0.016$ (**6b**) and $\Phi_{\text{D}} = 0.012$ (**6c**). Attempts to isolate the products formed upon illumination of compounds **6c** turned out to be unsuccessful. Further studies were performed to ensure that these compounds did not react with singlet oxygen. The photooxygenation of **6a** with 2 mol% of a diiodoBodipy photosensitizer under oxygen atmosphere and upon illumination with a green LED did not show any decomposition of the chromophore by ¹H NMR spectroscopy (see Supporting Information for further details). As a result, singlet oxygen would not be involved in the photobleaching process.

Phenalenone (**18,19**) and compounds **6a-c** showed a similar absorption profile between 300 and 450 nm but phenalenone was described as photostable while phenalenone-like compounds **6a-c** were unstable upon irradiation. Nevertheless, all these dyes are able to produce singlet oxygen by photosensitization (see results below).

Singlet oxygen generation. Singlet oxygen quantum yields (Φ_{Δ}) were determined by observing the 1270 nm emission of ¹O₂ of air-saturated samples excited at 355 nm (Table 4).

The compound **5a** showed the lowest singlet oxygen quantum yield values and this result is fully consistent with its higher fluorescence quantum yield (Table 3). On the other hand, the compounds **6a-c** displayed higher singlet oxygen quantum yields. Singlet-triplet energy gaps (ΔE_{ST}) have been computed at the excited state geometry for each investigated system in gas phase

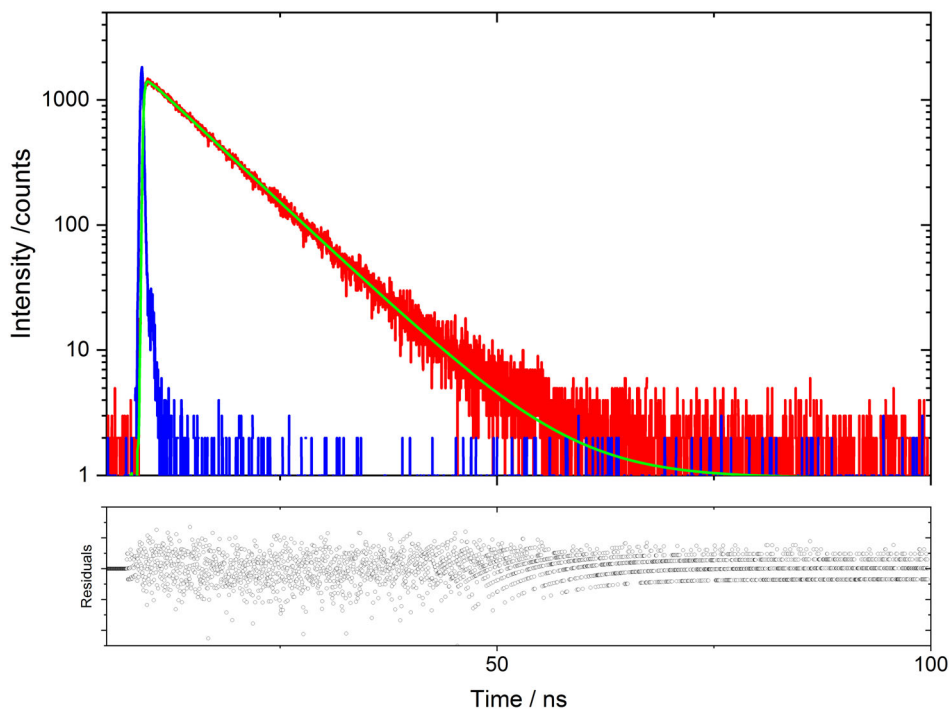


Figure 4. Emission decay of **5a** in acetonitrile at 520 nm ($\lambda_{\text{exc}} = 375$ nm) under air.

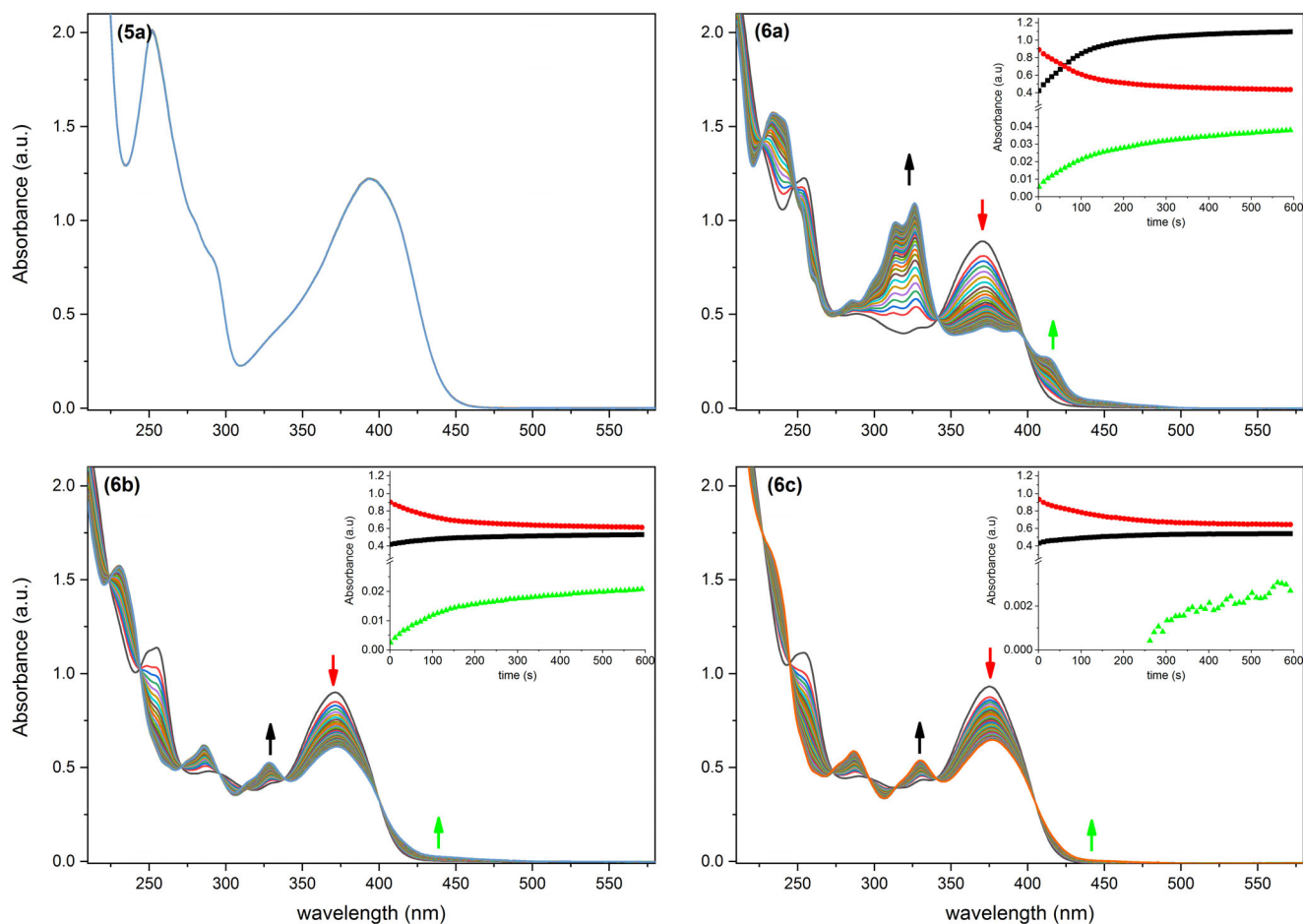


Figure 5. Evolution of the absorption spectra of an acetonitrile solution of **5a**, **6a-c** over a period of 10 min upon 365 nm irradiation. For compounds **6a-c**, the evolution of the absorbance *versus* time at three different wavelengths has been displayed.

Table 4. Singlet oxygen generation quantum yields, determined using phenalene as actinometer. $\lambda_{\text{exc}} = 355$ nm. Singlet oxygen generation quantum yields after 15 min of irradiation at 365 nm are shown in brackets. Computed ΔE_{ST} (eV) on optimized excited state geometry in gas phase at the SCS-CC2 level of theory and SOC values were obtained at the SMD(acetonitrile)-M06-2X/Def2-DZVP; SOC not yet implemented for ECP in case of **6c**.

Compound	Experimental $\Phi_{\Delta, \text{air}}$		Computed properties (MeCN)	
	MeCN	CHCl_3	ΔE_{ST} (eV)	SOC (cm^{-1})
5a	0.273	0.227	0.85	0.33
6a	0.329 (0.444)	0.342 (0.554)	0.15	0.38
6b	0.364 (0.700)	0.412 (0.618)	0.15	0.40
6c	0.448 (0.468)	0.621 (0.632)	0.18	–

using SCS-CC2 method known to be accurate for such gap (56). The compound **5a** presents the highest gap value (>0.2 eV) and the lowest SOC (0.33 cm^{-1}) while the oxidized from (**6a-c**) are characterized by a much lower ΔE_{ST} value (<0.2 eV) and a larger SOC values than **5a**. Therefore ΔE_{ST} being much larger for **5a** than for **6a-c** the intersystem crossing constant is smaller for **5a** than for **6a-c**, as experimentally observed. Additionally, as mentioned previously, a clear effect of the presence of a halogen with increasing atomic number correlates with an increase in the

capability of generating excited oxygen (53–55). In summary, the presence of heavy atoms in the core of a photosensitizer is important for the production of singlet oxygen owing to a favored intersystem crossing to the triplet state.

As mentioned previously, compounds **6a-c** were prone to photobleaching upon illumination at 365 nm (Fig. 4). Regardless of the solvent, singlet oxygen quantum yields after 15 min of irradiation at 365 nm were higher than the parent compound **6**. Therefore, photoproducts of compound **6a** and **6b**, in both solvents, are better generators of singlet oxygen, while the iodine substituted compound, **6c**, yields photoproducts with a comparable propensity to generate excited oxygen.

CONCLUSIONS

In summary, we have prepared a new family of photosensitizers derived from the pyrroloquinolone framework. The key steps involved an aminocatalyzed process to construct the pyrroloquinoline framework and its oxidation with 2,3-dichloro-5,6-dicyano-1,4-benzoquinone (DDQ) in the presence of water. Upon oxidation, a marked decrease of fluorescence efficiency of the chromophores was observed and simultaneously, an increase of the photoproduction of singlet oxygen was confirmed by observing the 1270 nm emission of $^1\text{O}_2$. Computational investigations showed a reduction of the energy gap between the singlet and

triplet excited states (ΔE_{ST}) and a higher value of SOC for the oxidized form which could explain the intersystem crossing efficiency of the photosensitizers **6**. As expected, the incorporation of halogen atoms with higher atomic numbers led to an increase of the singlet oxygen quantum yield. In spite of a low photostability, the best results were obtained with the iodine-containing photosensitizer owing to a strongest intersystem crossing. Work is in progress to increase the photostability of the photosensitizers and to enhance the singlet oxygen photoproduction.

Acknowledgements—This work benefited from the support of the project CaROS (ANR-18-CE07-0013-01) of the French National Research Agency (ANR). In particular, P.D.B. thanks ANR for a Ph.D. grant. We also thank Université de Nantes and CNRS for financial support. A.D.L. acknowledges the CCIPL computational center installed in Nantes for allocation of computational time as well as D. Jacquemin and M. Bousquet for fruitful discussions. The authors greatly acknowledge J. Hémez and L. Arzel (AMaCC platform, CEISAM UMR CNRS 6230, Nantes Université) for their mass spectrometry analytical contributions to this work. This work includes NMR experiments carried out on the CEISAM NMR platform.

SUPPORTING INFORMATION

Additional supporting information may be found online in the Supporting Information section at the end of the article:

Methods S1. Photostability experiment of **6a** under photooxygenation conditions.

Data S1. ^1H and ^{13}C NMR spectra of products.

Data S2. Full characterization of **6a**.

Data S3. Representation of GS geometries and xyz coordinates for **5a** and **6a-c**.

Figure S1. Ground state geometries of **5a** and **6b** along with electronic density difference plots.

Figure S2. Representation of the ground state (S_0) and excited state (S_1) geometries of **5a** and **6a-c**.

Table S1. Computed absorption and emission λ_{max} (oscillator strengths in parenthesis) at the M06-2X-6-311 + G(2d,p) level of theory using PCM solvent (MeCN) and the cLR² to account for the electronic response of the solvent.

REFERENCES

- Verhoeven, J. W. (1996) Glossary of terms used in photochemistry (IUPAC recommendations 1996). *Pure Appl. Chem.* **68**, 2223–2286.
- Nonell, S. and C. Flors (eds) (2016) *Singlet Oxygen: Applications in Biosciences and Nanosciences*, Vol. **1** and **2**. The Royal Society of Chemistry, Cambridge, UK.
- Pibiri, I., S. Buscemi, A. Palumbo Piccionello and A. Pace (2018) Photochemically produced singlet oxygen: Applications and perspectives. *ChemPhotoChem* **2**, 535–547.
- Ogilby, P. R. (2010) Singlet oxygen: There is indeed something new under the sun. *Chem. Soc. Rev.* **39**, 3181–3209.
- Schweitzer, C. and R. Schmidt (2003) Physical mechanisms of generation and deactivation of singlet oxygen. *Chem. Rev.* **103**, 1685–1758.
- DeRosa, M. C. and R. J. Crutchley (2002) Photosensitized singlet oxygen and its applications. *Coord. Chem. Rev.* **233–234**, 351–371.
- Zamadar, M. and A. Greer (2009) Singlet oxygen as a reagent in organic synthesis. In *Handbook of Synthetic Photochemistry*, (Edited by A. Albini and M. Fagnoni), pp. 353–386. Wiley-VCH Verlag GmbH & Co. KGaA, Weinheim.
- Ghogare, A. A. and A. Greer (2016) Using singlet oxygen to synthesize natural products and drugs. *Chem. Rev.* **116**, 9994–10034.
- Mauger, A., J. Farjon, P. Nun and V. Coeffard (2018) One-pot synthesis of functionalized fused furans via a BODIPY-catalyzed domino photooxygenation. *Chem. Eur. J.* **24**, 4790–4793.
- Péault, L., P. Nun, E. Le Grogneq and V. Coeffard (2019) Multicatalytic dearomatization of phenols into epoxyquinols via a photooxygenation process. *Chem. Commun.* **55**, 7398–7401.
- Péault, L., A. Planchat, P. Nun, E. Le Grogneq and V. Coeffard (2021) Atom economical photocatalytic oxidation of phenols and site-selective epoxidation toward Epoxyquinols. *J. Org. Chem.* **86**, 18192–18203.
- Nguyen, V.-N., Z. Zhao, B. Z. Tang and J. Yoon (2022) Organic photosensitizers for antimicrobial phototherapy. *Chem. Soc. Rev.* **51**, 3324–3340.
- Pham, T. C., V.-N. Nguyen, Y. Choi, S. Lee and J. Yoon (2021) Recent strategies to develop innovative photosensitizers for enhanced photodynamic therapy. *Chem. Rev.* **121**, 13454–13619.
- Lan, M., S. Zhao, W. Liu, C.-S. Lee, W. Zhang and P. Wang (2019) Photosensitizers for photodynamic therapy. *Adv. Healthc. Mater.* **8**, 1900132.
- Lacombe, S. and T. Pigot (2016) Materials for selective photooxygenation vs. photocatalysis: Preparation, properties and applications in environmental and health fields. *Cat. Sci. Technol.* **6**, 1571–1592.
- Zhao, X., J. Liu, J. Fan, H. Chao and X. Peng (2021) Recent progress in photosensitizers for overcoming the challenges of photodynamic therapy: From molecular design to application. *Chem. Soc. Rev.* **50**, 4185–4219.
- Sasikumar, D., A. T. John, J. Sunny and M. Hariharan (2020) Access to the triplet excited states of organic chromophores. *Chem. Soc. Rev.* **49**, 6122–6140.
- Flors, C. and S. Nonell (2006) Light and singlet oxygen in plant defense against pathogens: Phototoxic Phenalenone Phytoalexins. *Acc. Chem. Res.* **39**, 293–300.
- Schmidt, R., C. Tanielian, R. Dunsbach and C. Wolff (1994) Phenalenone, a universal reference compound for the determination of quantum yields of singlet oxygen O₂(¹Δ_g) sensitization. *J. Photochem. Photobiol. A* **79**, 11–17.
- Daza, M. C., M. Doerr, S. Salzmänn, C. M. Marian and W. Thiel (2009) Photophysics of phenalenone: Quantum-mechanical investigation of singlet-triplet intersystem crossing. *Phys. Chem. Chem. Phys.* **11**, 1688–1696.
- Rivas Aiello, M. B., G. C. Lavorato, J. C. Azcárate, J. M. Orozco-Henao, P. Mendoza Zélis, C. J. Cobos, M. H. Fonticelli, D. O. Mártire and C. Vericat (2022) Magnetic nanoparticle-polymer composites loaded with hydrophobic sensitizers for Photodegradation of azoic dyes. *ACS Appl. Nano Mater* **5**, 7460–7470.
- Godard, J., D. Gibbons, S. Leroy-Lhez, R. M. Williams, N. Villandier, T.-S. Ouk, F. Brégier and V. Sol (2021) Development of Phenalenone-Triazolium salt derivatives for aPDT: Synthesis and antibacterial screening. *Antibiotics* **10**, 626.
- Bresolí-Obach, R., I. Gispert, D. G. Peña, S. Boga, Ó. Gulias, M. Agut, M. E. Vázquez and S. Nonell (2018) Triphenylphosphonium cation: A valuable functional group for antimicrobial photodynamic therapy. *J. Biophotonics* **11**, e201800054.
- Späth, A., C. Leibl, F. Cieplik, K. Lehner, J. Regensburger, K.-A. Hiller, W. Bäuml, G. Schmalz and T. Maisch (2014) Improving photodynamic inactivation of bacteria in dentistry: Highly effective and fast killing of Oral key pathogens with novel tooth-colored type-II photosensitizers. *J. Med. Chem.* **57**, 5157–5168.
- Lazzaro, A., M. Corominas, C. Martí, C. Flors, L. R. Izquierdo, T. A. Grillo, J. G. Luis and S. Nonell (2004) Light- and singlet oxygen-mediated antifungal activity of phenylphenalenone phytoalexins. *Photochem. Photobiol. Sci.* **3**, 706–710.
- Kaye, E. G., K. Kailass, O. Sadovski and A. A. Beharry (2021) A green-absorbing, red-fluorescent Phenalenone-based photosensitizer as a Theranostic agent for photodynamic therapy. *ACS Med. Chem. Lett.* **12**, 1295–1301.
- Jing, Y., Q. Xu, M. Chen and X. Shao (2019) Pyridone-containing phenalenone-based photosensitizer working both under light and in the dark for photodynamic therapy. *Bioorg. Med. Chem.* **27**, 2201–2208.

28. De Bonfils, P., E. Verron, C. Sandoval-Altamirano, P. Jaque, X. Moreau, G. Gunther, P. Nun and V. Coeffard (2020) Unusual oxidative Dealkylation strategy toward functionalized Phenalenones as singlet oxygen photosensitizers and Photophysical studies. *J. Org. Chem.* **85**, 10603–10616.
29. Giardinetti, M., X. Moreau, V. Coeffard and C. Greck (2015) Aminocatalyzed cascade synthesis of enantioenriched 1,7-annulated indoles from indole-7-carbaldehyde derivatives and α,β -unsaturated aldehydes. *Adv. Synth. Catal.* **357**, 3501–3506.
30. Moudam, O., F. Ajamaa, A. Ekouaga, H. Mamlouk, U. Hahn, M. Holler, R. Welter and J.-F. Nierengarten (2007) A new synthetic route for the preparation of 1,10-Phenanthroline derivatives. *Eur. J. Org. Chem.* **2007**, 417–419.
31. de Guidi, G., G. Bracchitta and A. Catalfo (2011) Photosensitization reactions of fluoroquinolones and their biological consequences. *Photochem. Photobiol.* **87**, 1214–1229.
32. Martinez, L. J., R. H. Sik and C. F. Chignell (1998) Fluoroquinolone antimicrobials: Singlet oxygen, superoxide and phototoxicity. *Photochem. Photobiol.* **67**, 399–403.
33. Layek, M., M. A. Reddy, A. V. Dhanunjaya Rao, M. Alvala, M. K. Arunasree, A. Islam, K. Mukkanti, J. Iqbal and M. Pal (2011) Transition metal mediated construction of pyrrole ring on 2,3-dihydroquinolin-4(1H)-one: Synthesis and pharmacological evaluation of novel tricyclic heteroarenes. *Org. Biomol. Chem.* **9**, 1004–1007.
34. Dorow, R. L., P. M. Herrinton, R. A. Hohler, M. Y. Maloney, M. A. Mauragis, W. E. McGhee, J. A. Moeslein, J. W. Strohbach and M. F. Veley (2006) Development of an efficient synthesis of the Pyrroloquinolone PHA-529311. *Org. Process. Res. Dev.* **10**, 493–499.
35. Bass, R. J., R. C. Koch, H. C. Richards and J. E. Thorpe (1981) Tricyclic amides: A new class of systemic fungicides active against rice blast disease. *J. Agric. Food Chem.* **29**, 576–579.
36. Via, L. D., G. Marzaro, A. Ferrarese, O. Gia and A. Chilin (2014) Pyrroloquinolinone-based dual topoisomerase III inhibitor. *Eur. J. Med. Chem.* **77**, 103–109.
37. Lucas, S., M. Negri, R. Heim, C. Zimmer and R. W. Hartmann (2011) Fine-tuning the selectivity of aldosterone synthase inhibitors: Structure–activity and structure–selectivity insights from studies of Heteroaryl substituted 1,2,5,6-Tetrahydropyrrolo[3,2,1-ij]quinolin-4-one derivatives. *J. Med. Chem.* **54**, 2307–2319.
38. Jones, S. G., A. R. Young and T. G. Truscott (1993) Singlet oxygen yields of furocoumarins and related molecules – The effect of excitation wavelength. *J. Photochem. Photobiol. B Biol.* **21**, 223–227.
39. Hartline, C. B., E. A. Harden, S.-L. Williams-Aziz, N. L. Kushner, R. J. Brideau and E. R. Kern (2005) Inhibition of herpesvirus replication by a series of 4-oxo-dihydroquinolines with viral polymerase activity. *Antivir. Res.* **65**, 97–105.
40. Nieman, J. A., S. K. Nair, S. E. Heasley, B. L. Schultz, H. M. Zerth, R. A. Nugent, K. Chen, K. J. Stephanski, T. A. Hopkins, M. L. Knechtel, N. L. Oien, J. L. Wieber and M. W. Wathen (2010) Modifications of C-2 on the pyrroloquinoline template aimed at the development of potent herpesvirus antivirals with improved aqueous solubility. *Bioorg. Med. Chem. Lett.* **20**, 3039–3042.
41. Mphahlele, M. J., M. M. Maluleka, S. T. Leruoibaaki and Y. S. Choong (2020) Synthesis, crystal structure, cytotoxicity and evaluation of the 6-oxo-6H-pyrrolo[3,2,1-ij]quinoline-5-carbaldehydes for inhibitory effect against protein kinases (VEGFR-2 and EGFR) and cyclooxygenase-2 (COX-2) activities. *J. Mol. Struct.* **1222**, 128907.
42. Kochnev, A. I., I. I. Oleinik, I. V. Oleinik, S. S. Ivanchev and G. A. Tolstikov (2007) Design of schiff base-like postmetallocene catalytic systems for polymerization of olefins: IV. Synthesis of 2-(aryliminomethyl)-pyrrole and 7-(aryliminomethyl)indole derivatives containing cycloalkyl substituents. *Russ. J. Org. Chem.* **43**, 571–575.
43. Sandoval-Altamirano, C., J. R. De la Fuente, E. Berrios, S. A. Sanchez, N. Pizarro, J. Morales and G. Gunther (2018) Photophysical characterization of hydroxy and ethoxy phenalenone derivatives. *J. Photochem. Photobiol. A Chem.* **353**, 349–357.
44. Frisch, M. J., G. W. Trucks, H. B. Schlegel, G. E. Scuseria, M. A. Robb, J. R. Cheeseman, G. Scalmani, V. Barone, G. A. Petersson, H. Nakatsuji, X. Li, M. Caricato, A. V. Marenich, J. Bloino, B. G. Janesko, R. Gomperts, B. Mennucci, H. P. Hratchian, J. V. Ortiz, A. F. Izmaylov, J. L. Sonnenberg, D. Williams-Young, F. Ding, F. Lipparini, F. Egidi, J. Goings, B. Peng, A. Petrone, T. Henderson, D. Ranasinghe, V. G. Zakrzewski, J. Gao, N. Rega, G. Zheng, W. Liang, M. Hada, M. Ehara, K. Toyota, R. Fukuda, J. Hasegawa, M. Ishida, T. Nakajima, Y. Honda, O. Kitao, H. Nakai, T. Vreven, K. Throssell, J. A. Montgomery Jr., J. E. Peralta, F. Ogliaro, M. J. Bearpark, J. J. Heyd, E. N. Brothers, K. N. Kudin, V. N. Staroverov, T. A. Keith, R. Kobayashi, J. Normand, K. Raghavachari, A. P. Rendell, J. C. Burant, S. S. Iyengar, J. Tomasi, M. Cossi, J. M. Millam, M. Klene, C. Adamo, R. Cammi, J. W. Ochterski, R. L. Martin, K. Morokuma, O. Farkas, J. B. Foresman and D. J. Fox (2016) *Gaussian 16, Revision A.03*. Gaussian, Inc., Wallingford, CT.
45. Zhao, Y. and D. G. Truhlar (2008) The M06 suite of density functionals for main group thermochemistry, thermochemical kinetics, noncovalent interactions, excited states, and transition elements: Two new functionals and systematic testing of four M06-class functionals and 12 other functionals. *Theor. Chem. Accounts* **120**, 215–241.
46. Tomasi, J., B. Mennucci and R. Cammi (2005) Quantum mechanical continuum solvation models. *Chem. Rev.* **105**, 2999–3094.
47. Caricato, M., B. Mennucci, J. Tomasi, F. Ingrosso, R. Cammi, S. Corni and G. Scalmani (2006) Formation and relaxation of excited states in solution: A new time dependent polarizable continuum model based on time dependent density functional theory. *J. Chem. Phys.* **124**, 124520.
48. Neese, F., F. Wennmohs, U. Becker and C. Riplinger (2020) The ORCA quantum chemistry program package. *J. Chem. Phys.* **152**, 224108.
49. Neese, F. (2005) Efficient and accurate approximations to the molecular spin-orbit coupling operator and their use in molecular g-tensor calculations. *J. Chem. Phys.* **122**, 034107.
50. Bartoli, G., G. Palmieri, M. Bosco and R. Dalpozzo (1989) The reaction of vinyl grignard reagents with 2-substituted nitroarenes: A new approach to the synthesis of 7-substituted indoles. *Tetrahedron Lett.* **30**, 2129–2132.
51. Sharma, S. and A. Sharma (2019) Recent advances in photocatalytic manipulations of rose Bengal in organic synthesis. *Org. Biomol. Chem.* **17**, 4384–4405.
52. Xu, T.-T., T.-S. Jiang, X.-L. Han, Y.-H. Xu and J.-P. Qiao (2018) Modular synthesis of (E)-cinnamaldehydes directly from allylarenes via a metal-free DDQ-mediated oxidative process. *Org. Biomol. Chem.* **16**, 5350–5358.
53. Piskorz, J., W. Porolnik, M. Kucinska, J. Dlugaszewska, M. Murias and J. Mielcarek (2021) BODIPY-based photosensitizers as potential anticancer and antibacterial agents: Role of the positive charge and the heavy atom effect. *ChemMedChem* **16**, 399–411.
54. Bassan, E., A. Gualandi, P. G. Cozzi and P. Ceroni (2021) Design of BODIPY dyes as triplet photosensitizers: Electronic properties tailored for solar energy conversion, photoredox catalysis and photodynamic therapy. *Chem. Sci.* **12**, 6607–6628.
55. Podsiadly, R., A. M. Szymczak and K. Podemska (2009) The synthesis of novel, visible-wavelength, oxidizable polymerization sensitizers based on the 8-halogeno-5,12-dihydroquinoxalino[2,3-b]quinoxaline skeleton. *Dyes Pigments* **82**, 365–371.
56. Pershin, A., D. Hall, V. Lemaur, J.-C. Sancho-Garcia, L. Muccioli, E. Zysman-Colman, D. Beljonne and Y. Olivier (2019) Highly emissive excitons with reduced exchange energy in thermally activated delayed fluorescent molecules. *Nat. Commun.* **10**, 597.